LETTERS

Charge self-regulation upon changing the oxidation state of transition metals in insulators

Hannes Raebiger[1], Stephan Lany[1] & Alex Zunger[1]

Transition-metal atoms embedded in an ionic or semiconducting crystal can exist in various oxidation states that have distinct signatures in X-ray photoemission spectroscopy and 'ionic radii' which vary with the oxidation state of the atom. These oxidation states are often tacitly associated with a physical ionization of the transition-metal atoms[1,2]—that is, a literal transfer of charge to or from the atoms. Physical models have been founded on this charge-transfer paradigm[3–6], but first-principles quantum mechanical calculations show only negligible changes in the local transition-metal charge[7–12] as the oxidation state is altered. Here we explain this peculiar tendency of transition-metal atoms to maintain a constant local charge under external perturbations in terms of an inherent, homeostasis-like negative feedback. We show that signatures of oxidation states and multivalence—such as X-ray photoemission core-level shifts, ionic radii and variations in local magnetization—that have often been interpreted as literal charge transfer[3,4,13–16] are instead a consequence of the negative-feedback charge regulation.

Classic inorganic chemistry of transition-metal (TM) coordination compounds and semiconductors[1,2] tacitly assumes that when the total charge of the compound is altered (for example through oxidation/reduction, carrier injection, chemical doping or decomposition of the compound), most of the changes are accommodated by a change in the charge of the TM ion. For example, when $LiTMO_2$ is delithiated, the original TM^{3+} ion is thought to be converted to a TM^{4+} ion. Although this concept of formal charges and changes therein provides useful bookkeeping, in many cases these formal charge states have been considered physical entities, capable of physical (for example point-ion Coulomb) interactions. Further examples of this concept include (1) the attribution[3] of a spatial ordering of inequivalent Mn atoms in $RMnO_3$ manganites (where R represents La, …, Tb or Dy) to Coulomb ordering of point charges associated with the formal charges of Mn^{4+} and Mn^{3+} ions; (2) the assumption that photoemission core-level shifts of TM ions within compounds reflect the physical charge of the TM ion itself[3,4]; and (3) the view that the variation of TM–ligand bond length with oxidation state[5] ('ionic radii') of TMs is a reflection of an explicit charge transfer between the TM and the ligand.

To address this concept of charge transfer on a general level, we specifically study multiple-charge configurations of isolated TM atoms in representative host materials. These include the archetypal ionic and covalent compounds, respectively MgO and GaAs, as well as an intermediate case involving *d* electrons, namely Cu_2O. We illustrate the negative charge feedback in terms of a simple energy-level model[7,8,17] (Fig. 1). Here the isolated TM(*d*) orbitals occupied by *n* electrons split into crystal field levels with irreducible representations γ (for example, for cubic symmetry these levels have the representations $\gamma = t$ (triply degenerate) and $\gamma = e$ (doubly degenerate)). The crystal field levels TM(γ) (Fig. 1a, left) that have the same representation and spin as the anion dangling bond levels DB(γ) of the cation vacancy (Fig. 1a, right) interact with these DB(γ) levels, and the interaction causes bonding levels to form below the valence band maximum and antibonding levels to form inside the band gap (Fig. 1a, centre). When the energy of the TM(γ) level is lower than that of the DB(γ) level, the bonding level occurs as a crystal field resonance (CFR) with a strong TM character and the antibonding level occurs as a dangling bond hybrid (DBH) formed mostly of the ligand *p* orbitals, and vice versa when the energy of the TM(γ) level is higher than that of the DB(γ) level, as illustrated in Fig. 1a, b.

Figure 1b shows how energy levels evolve when the system in Fig. 1a is doped with an electron. The level occupancy of the TM-induced hybrid states increases, and the system charge q becomes $q' = q - 1$ (Fig. 1b). Such charge doping causes the TM levels and, consequently, the bonding and antibonding hybrid levels to shift up in energy by means of a negative feedback: in Fig. 1a the isolated TM(γ^n) orbital level (*n* denotes the electron occupancy) is lower in energy than the host DB(γ) level, so the bonding level occurs as a crystal field resonance, γ^{CFR}, and the antibonding level occurs as a dangling bond hybrid, γ^{DBH}, just above the valence band maximum. In Fig. 1b the atomic TM level, TM(γ^{n+1}), is higher in energy than the DB(γ) level, and the CFR occurs as the gap level whereas the DBH occurs as resonant state inside the host bands. Thus, the relative weight of the bonding levels shifts towards the ligands, and this negative feedback causes a depopulation of TM charge in the bonding states, counterbalancing the increase in the antibonding gap-level charge. As a result of this self-regulated response, the net local charge at the TM site remains approximately constant. In this model, the formal oxidation state does not reflect the local charge at the TM site, but rather the occupancy of the respective crystal field levels (for example e^2t^3 for Mn^0_{Ga} in GaAs, see Supplementary Information section A).

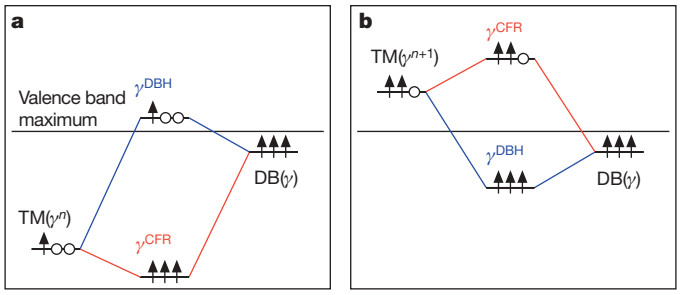

Figure 1 | Energy-level diagrams for TM–host interaction. a, System charge, q; **b**, system charge, $q - 1$. In each panel, the free-TM-atom orbital with irreducible representation γ (left-hand side) interacts with a host dangling bond level with the same representation (right-hand side), forming two hybrid levels (centre), namely the crystal field resonance level γ^{CFR} and a dangling bond hybrid level γ^{DBH}. The arrows indicate spin-up electrons occupying the level, and the circles indicate unoccupied states.

[1]National Renewable Energy Laboratory, Golden, Colorado 80401, USA.

Note that although the electronic charge associated with the CFR level is localized more on the TM site than on the ligands, and that of the DBH level is localized more on the ligands than on the TM site, both levels are hybrid states whose relative weight changes upon adding or removing electrons, owing to the negative charge feedback mechanism described in this work.

To quantify the TM response to changes in global charge, we calculate *ab initio* the change in total energy when the occupation of the antibonding gap level is changed, corresponding to a change in system charge from q to q'. These transition energies (donor or acceptor 'levels') are calculated, with respect to the valence band maximum ε_v, as

$$\varepsilon(q/\,q') = \frac{E(q') - E(q)}{q - q'} - \varepsilon_v$$

where $E(q)$ is the total energy of the system in charge state q, and by convention the slash in the argument of $\varepsilon(q/\,q')$ serves to indicate transition between charge states (not division of the charges). These transition energies are given in Figs 2 and 3. We see that all of the considered 3*d* impurities have such transition levels in the host crystal band gap, consistent also with experiment[18]. The effective Mott–Hubbard U

$$U = E(q+1) + E(q-1) - 2E(q) = \varepsilon(q-1/\,q) - \varepsilon(q/\,q+1) \quad (1)$$

is defined as the difference between two successive 'transition energies', for example $\varepsilon(0/-1) - \varepsilon(+1/0)$.

Figures 2 and 3 show that for charge states q that are stable in the gap, U ranges roughly from 0.4 to 3.3 eV. This 'system U' characterizing the combined host–impurity system is one to two orders smaller than the Mott–Hubbard U for the free TM atom, which is $U_{atom} \approx 30$ eV (Table 1). The existence of multiple charge configurations within a small semiconductor band gap with this large reduction in U was explained by Haldane and Anderson[19] by changes in hybridization. From the point of view of polarization theory, U_d, which describes a TM(d) level embedded in an insulating system, was empirically found[6] to be approximately described by the relation $U_d = U_{atom}(1 - 1/\varepsilon_{eff})e^2/R$, where e is the electron charge, ε_{eff} is an effective constant for dielectric screening and R is the ionic radius (tabulated in ref. 5). Such polarization and screening effects on U are naturally included in our density-functional calculations, but we emphasize here the importance of the non-rigid electronic level transformation (Fig. 1). This usually receives little attention in ionic systems, where the change of gap-level occupation (increase in Q_{gap}; see charge definitions below) is often interpreted as a literal (rigid-band-like) TM ionization (increase in Q_{tot})[3,4,13–16].

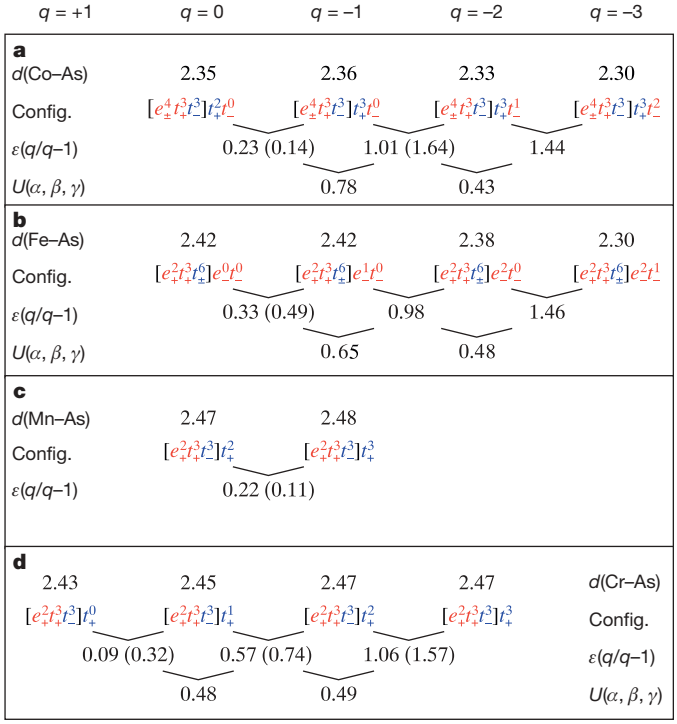

Figure 2 | Properties of GaAs:TM systems, as functions of stable system charge q. **a**, GaAs:Co; **b**, GaAs:Fe; **c**, GaAs:Mn; **d**, GaAs:Cr. In each panel we show bond lengths d(TM–As) (Å; first line), single-particle level configurations (second line), transition energies $\varepsilon(q/\,q-1)$ (eV; third line) and Coulomb energies $U(\alpha, \beta, \gamma)$ (eV; fourth line). The single-particle levels resonant in the valence band are shown in square brackets, CFRs are shown in red and DBHs are shown in blue. The transition energies are given for successive charge states q and $q-1$, and the Coulomb energies $U(\alpha, \beta, \gamma)$ corresponding to single-particle level configurations α, β and γ for successive transition levels. Experimental values for the transition levels[18] are given in parentheses.

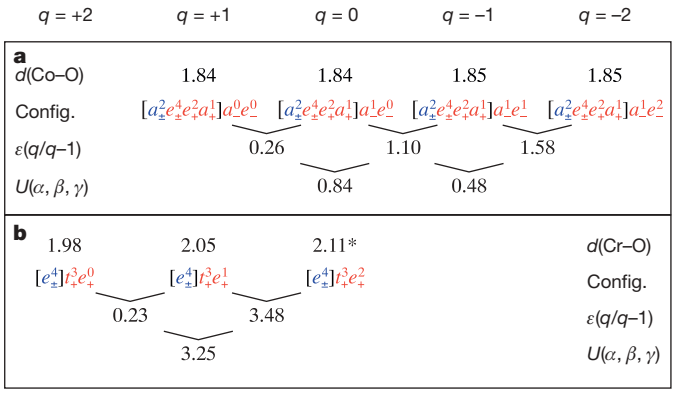

Figure 3 | Properties of Cu_2O:Co and MgO:Cr, as functions of stable system charge q. **a**, Cu_2O:Co; **b**, MgO:Cr. As in Fig. 2, with bond lengths d(Co–O) (**a**) and d(Cr–O) (**b**). We note that the charge-neutral state for MgO:Cr (denoted with an asterisk) is Jahn–Teller distorted: four O ions have a Cr–O distance of 2.11 Å, whereas two O ions relax outwards and have a Cr–O distance of 2.29 Å.

Although there is no unambiguous way to determine an ionic charge in a solid, the ionization of an atom (that is, a literal charge transfer) should be reflected by a change in the integrated electronic charge within a fixed region of space around the atomic site. We calculate the charge Q_{tot}, due to all occupied levels below the Fermi energy inside a sphere of radius R centred at the atomic position of the TM for system charge q, as[1]

$$Q_{tot}(q) = \int_0^R \mathrm{d}r\ \rho(r) = \sum_i^{occ.} \int_0^R \mathrm{d}r\ \psi_i^2$$

where the sum is taken over all occupied levels, ψ_i is the wavefunction projected on TM(d) orbitals, ρ is the charge density and R is chosen as 1.3 Å. The total charge Q_{tot} is further decomposed into the charge Q_{gap} corresponding to the antibonding gap level (summing over all occupied gap levels) and the charge Q_{VB} corresponding to the bonding TM states (summing over all levels below the valence band maximum) resonant within the valence band ($Q_{tot} = Q_{gap} + Q_{VB}$):

Table 1 | Mott–Hubbard U (eV) for the free ions, calculated as defined in equation (1)

TM	$U(d^5, d^4, d^3)$	$U(d^4, d^3, d^2)$	$U(d^3, d^2, d^1)$
Co	27.3	29.5	32.9
Fe	26.8	27.1	27.5
Mn	28.0	23.8	29.3
Cr	25.2	29.5	22.3

The free-atom total energies are calculated using the same GGA-PBE functional as used in the host–impurity calculations.

$$Q_{\mathrm{gap}}(q) = \sum_{i}^{\mathrm{gap}} \int_0^R \mathrm{d}r\, \psi_i^2$$

$$Q_{\mathrm{VB}}(q) = \sum_{i}^{\mathrm{VB}} \int_0^R \mathrm{d}r\, \psi_i^2$$

Figure 4 shows the integrated charge quantities Q_{tot}, Q_{gap} and Q_{VB} as functions of electronic configuration, or system charge q. Increasing the system charge by populating the antibonding gap levels (Fig. 1) causes the corresponding gap-level charge Q_{gap} around the TM site to increase by $0.2e$–$1e$ per one electron increase in q. In a naive rigid-band picture the total charge Q_{tot} around the TM is expected to increase by the same amount as Q_{gap} increases. However, owing to the negative feedback (in the self-consistent calculation), the charge Q_{VB} around the TM, contributed by the bonding levels resonant in the valence band (Fig. 1), decreases by the amount Q_{gap} increases, keeping the total charge Q_{tot} around the TM almost unchanged. Consequently, for all $3d$ TMs studied in GaAs, Cu_2O and MgO, the total charge inside the TM-centred sphere changes by no more than $0.1e$ when the gap level is occupied or vacated by one electron.

The negative feedback causing the decrease in the charge Q_{VB} upon an increase of Q_{gap} is illustrated in terms of the energy-level shifts shown in Fig. 1a, b: when charge is added to the system, the TM(γ) free-atom levels, together with the corresponding bonding and antibonding levels of the combined system, are shifted to higher energies. Thus, the bonding level becomes more localized on the anion dangling bond, yielding a smaller contribution to the charge around the TM site. The orbital energy levels TM(γ) shift so as to balance out any increase in the charge of the antibonding gap level by 'leaking' charge from the bonding levels to the neighbouring anion sites (which may further leak charge to more distant neighbours). To illustrate this charge regulation, we show in Fig. 5 the spatial redistribution of charge density. We plot the difference in charge density ρ corresponding to the addition of one electron to the charge-neutral state of Mn in GaAs ($\Delta\rho = \rho(0) - \rho(-1)$; Fig. 5a), and to the charge-+1 states of Co in Cu_2O and Cr in MgO ($\Delta\rho = \rho(+1) - \rho(0)$; Fig. 5b, c). In all these cases, we find a decrease (shown in red) and an increase (shown in blue) in charge density around the TM site that tend to cancel each other out. The spatial shapes of the charge density differences correspond to the expected spatial shapes of the gap level symmetries (t, a and e for GaAs:Mn, Cu_2O:Co and MgO:Cr, respectively), and the increase and decrease have the spatial shape of antibonding and bonding levels, respectively. Thus, the increase in Q_{gap} and concomitant decrease in Q_{VB} shown in Fig. 4 can indeed be identified as an increase in antibonding and a decrease in bonding level charges, as suggested by the model in Fig. 1.

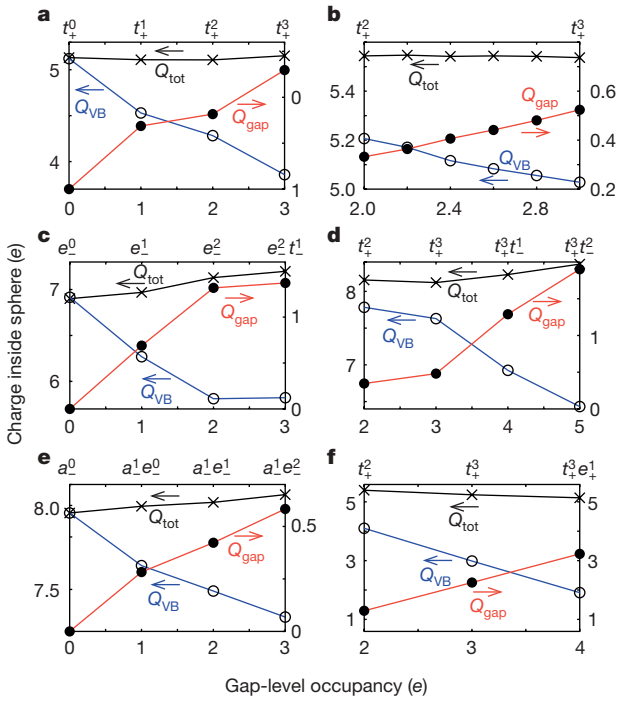

Figure 4 | Integrated charge inside the TM-centred sphere. **a**, GaAs:Cr; **b**, GaAs:Mn; **c**, GaAs:Fe; **d**, GaAs:Co; **e**, Cu_2O:Co; **f**, MgO:Cr. The total charge Q_{tot} is decomposed into contributions from gap-level charge Q_{gap} (red) and from TM charge inside the valence band Q_{VB} (blue).

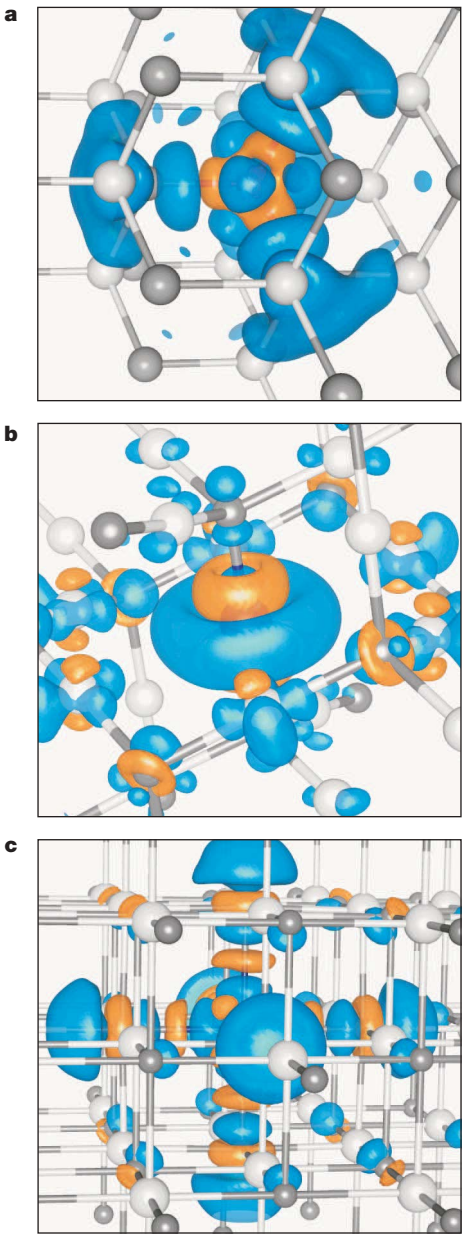

Figure 5 | Charge density differences. **a**, Difference between charge-−1 and charge-neutral states for GaAs:Mn; **b**, difference between charge-neutral and charge-+1 states for Cu_2O:Co; **c**, difference between charge-neutral and charge-+1 states for MgO:Cr. Cations and anions are shown as white and grey spheres, respectively. The blue and red isosurfaces respectively correspond to charge densities of $0.003e$ Å^{-3} and $-0.003e$ Å^{-3} (**a**), $0.01e$ Å^{-3} and $-0.01e$ Å^{-3} (**b**), and $0.015e$ Å^{-3} and $-0.015e$ Å^{-3}. We note that in each system, upon adding an electron, the blue and red isosurfaces respectively represent an increase and a decrease in the total charge density.

Even though there is no significant charge accumulation around the TM, different oxidation states may be assigned to the host–impurity system on the basis of the type of level being occupied. A change in gap-level occupation is accompanied by a change in the TM oxidation state only when the gap level is a CFR level (Fig. 1b), and not a DBH level (Fig. 1a). Similarly, a change in occupancy of a CFR level affects the local magnetization of the TM, whereas a change in occupancy of a DBH level affects the magnetization of host states instead. Furthermore, the change in spatial distribution of the charge density around the TM site upon changes in gap level occupancy (Fig. 5) influences all TM levels (even the presumably free-atom-like core levels), and can be observed as a core-level shift in an X-ray absorption experiment. (See also Supplementary Information section B.)

The changes in level occupation further affect the lattice relaxations, which for TM ions in oxides and sulphides were traditionally interpreted as ionic radii[5]. These ionic radii are based on the simple assumption that adding electrons to the TM ion increases its radius and removing electrons reduces its radius (order of magnitude of the change in TM ionic radius in an oxide host is typically 0.1 Å per electron added to system[5]). We find, however, by direct total-energy minimization of the TM–anion bond length when electrons are added to the MgO:Cr system (Fig. 3), an outward relaxation of nearest-neighbour O atoms of the same magnitude as reported in ref. 5, even when the local charge around the Cr atom does not increase (Fig. 4). Our results show that this increase in ionic radii upon reduction (adding electrons) simply reflects an increased occupation of the antibonding gap levels instead a of charge build-up at the TM atom itself. The magnitude of the inward/outward relaxation reflects the localization of the gap level; that is, when a level is strongly localized around the TM site, as it is for Cr in MgO, the associated local lattice relaxations are very large, whereas for less localized states, like the TM in GaAs or Co in Cu_2O, the lattice relaxations are smaller (Figs 2 and 3), because the antibonding level the occupation of which increases is more delocalized on extended host states.

The negative-feedback charge regulation is inherent to TMs, and thus occurs in virtually any TM coordination compound. Other than TM impurities in semiconductors[7,8], further examples include $CaMnO_3$[12], where Mn occupies two sites that are inequivalent in geometry but equivalent in charge, and the rehybridization of Co in Li_xCoO_2 upon removal of Li (ref. 9), or in Na_xCoO_2 upon removal of Na (ref. 20). This TM rehybridization associated with multiple oxidation states of the TM atom has been observed in manganites, nickelates, vanadates and so on, and is often falsely attributed to 'charge ordering'[3,13,14,16], that is, a model based on explicit charge transfer to or from the TM site. The self-regulating response, however, ensures that the net charge transfer Δq to or from the TM site is negligibly small ($|\Delta q| \ll 1$), contradicting any model based on assumptions of integer changes in ionization or 'charge disproportionation'. Instead, 'ordering' and 'disproportionation' in terms of different TM oxidation states (reflecting different orbital occupations) occurs at essentially constant TM charge, which is a consequence of the present negative charge-feedback mechanism.

METHODS SUMMARY

The TM atom embedded in a crystalline semiconductor or ionic host material was studied in supercells of 64–128 atoms with one host cation replaced with a 3*d* transition element. The global charge state was altered by occupying the energy levels appearing in the band gap by a different number of electrons, and a universal compensating background charge was added to maintain overall neutrality. Total energies and band structures were calculated within the generalized gradient approximation (GGA-PBE) to the density-functional formalism, as implemented in the VASP package[21,22]. Total energies and eigenvalues were corrected for potential alignment and image charges as described in the appendixes of ref. 23.

Received 15 December 2007; accepted 14 April 2008.

1. Wells, A. F. *Structural Inorganic Chemistry* (Clarendon, Oxford, UK, 1975).
2. Cotton, F. A. & Wilkinson, G. *Advanced Inorganic Chemistry* (Wiley, New York, 1988).
3. Goodenough, J. B. & Rivadulla, F. Bond-length fluctuations in transition-metal oxides. *Mod. Phys. Lett. B* **22,** 1057–1081 (2005).
4. Solomon, E. I., Hedman, B., Hodgson, K. O., Dey, A. & Szilagyi, R. K. Ligand K-edge X-ray absorption spectroscopy: covalency of ligand-metal bonds. *Coord. Chem. Rev.* **249,** 97–129 (2005).
5. Shannon, R. D. & Prewitt, C. T. Effective ionic radii in oxides and fluorides. *Acta Crystallogr. B* **25,** 925–946 (1969).
6. Koster, G., Geballe, T. H. & Moyzhes, B. Charge instabilities in the ionic model of metal oxides: importance of polarization energy. *Phys. Rev. B* **66,** 085109 (2002).
7. Zunger, A. & Lindefelt, U. Substitutional 3d impurities in silicon: a self-regulating system. *Solid State Commun.* **45,** 343–346 (1983).
8. Zunger, A. in *Solid State Physics* Vol. 39 (eds Seitz, F., Turnbull, D. & Ehrenreich, H.) 275–464 (Academic, New York, 1986).
9. Wolverton, C. & Zunger, A. First-principles prediction of vacancy order-disorder and intercalation battery voltages in Li_xCoO_2. *Phys. Rev. Lett.* **81,** 606–609 (1998).
10. Leonov, I., Yaresko, A. N., Antonov, V. N., Korotin, M. A. & Anisimov, V. I. Charge and orbital order in Fe_3O_4. *Phys. Rev. Lett.* **93,** 146404 (2004).
11. Jeng, H.-T., Guo, G. Y. & Huang, D. J. Charge-orbital ordering and Verwey transition in magnetite. *Phys. Rev. Lett.* **93,** 156403 (2004).
12. Luo, W. *et al.* Orbital-occupancy versus charge ordering and the strength of electron correlations in electron-doped $CaMnO_3$. *Phys. Rev. Lett.* **99,** 036402 (2007).
13. Ikeda, N. *et al.* Ferroelectricity from iron valence ordering in the charge-frustrated system $LuFe_2O_4$. *Nature* **436,** 1136–1138 (2005).
14. Angst, M. *et al.* Charge order with integer iron valence in Fe_2OBO_3. *Phys. Rev. Lett.* **99,** 086403 (2007).
15. Shim, J. H. & Lee, S. Coexistence of two different Cr ions by self-doping in half-metallic CrO_2 nanorods. *Phys. Rev. Lett.* **99,** 057209 (2007).
16. Mazin, I. I. *et al.* Charge ordering as alternative to Jahn-Teller distortion. *Phys. Rev. Lett.* **98,** 176406 (2007).
17. Mahadevan, P., Zunger, A. & Sarma, D. D. Unusual directional dependence of exchange energies in GaAs diluted magnetic semiconductors with Mn: Is the RKKY description relevant? *Phys. Rev. Lett.* **93,** 177201 (2004).
18. Clerjaud, B. Transition-metal impurities in III–V compounds. *J. Phys. C* **18,** 3615–3661 (1985).
19. Haldane, F. D. M. & Anderson, P. W. Simple model of multiple charge states of transition-metal impurities in semiconductors. *Phys. Rev. B* **13,** 2553–2559 (1976).
20. Karppinen, M., Asako, I., Motohashi, T. & Yamauchi, H. Oxygen nonstoichiometry and actual Co valence in $Na_xCoO_{2-\delta}$. *Phys. Rev. B* **71,** 092105 (2005).
21. Kresse, G. & Furthmüller, J. Efficient iterative schemes for *ab initio* total-energy calculations using a plane-wave basis set. *Phys. Rev. B* **54,** 11169–11186 (1996).
22. Kresse, G. & Joubert, D. From ultrasoft pseudopotentials to the projector augmented-wave method. *Phys. Rev. B* **59,** 1758–1775 (1999).
23. Persson, C., Zhao, Y. J., Lany, S. & Zunger, A. *n*-type doping in $CuInSe_2$ and $CuGaSe_2$. *Phys. Rev. B* **72,** 035211 (2005).

Supplementary Information is linked to the online version of the paper at www.nature.com/nature.

Acknowledgements H.R. thanks G. Trimarchi and J. Chan for discussions and for reading the manuscript. A.Z. thanks P. Mahadevan for interest in the early stages of this problem. This work was funded by the US Department of Energy, Office of Science, under NREL Contract No. DE-AC36-99GO10337.

Author Contributions H.R. carried out the calculations, analysed the results and wrote the paper. S.L. and A.Z. contributed to the design of the study, the analysis of results and the writing of the paper.

Author Information Reprints and permissions information is available at www.nature.com/reprints. Correspondence and requests for materials should be addressed to H.R. (hannes_raebiger@nrel.gov) or A.Z. (alex_zunger@nrel.gov).